# Breathing and heart rate estimation by FMCW radar system based on adaptive nonlinear filtering

Lazar Jugović
*University of Belgrade – School of Electrical Engineering and Novelic d.o.o*
Belgrade, Serbia
lazar.jugovic@novelic.com
& ORCID
0009-0003-3661-8996

Milan Stojanović
*University of Belgrade – School of Electrical Engineering and Novelic d.o.o*
Belgrade, Serbia
milan.stojanovic@novelic.com
& ORCID
0000-0002-1783-1615

Jelena Ćertić
*University of Belgrade – School of Electrical Engineering*
Belgrade, Serbia
certic@etf.rs
& ORCID
0000-0002-8732-6251

Milica Badža Atanasijević
*University of Belgrade – School of Electrical Engineering and Innovation Center of the School of Electrical Engineering in Belgrade*
Belgrade, Serbia
milica.badza@ic.etf.bg.ac.rs
& ORCID
0000-0002-5856-2626

Ivan Vajs
*Innovation Center of the School of Electrical Engineering in Belgrade*
Belgrade, Serbia
ivan.vajs@ic.etf.bg.ac.rs
& ORCID
0000-0001-7039-5384

Veljko Mihajlović
*Novelic d.o.o.*
Belgrade, Serbia
veljko.mihajlovic@novelic.com
& ORCID
0009-0003-1771-7278

Milica Janković
*University of Belgrade – School of Electrical Engineering*
Belgrade, Serbia
piperski@etf.rs
& ORCID
0000-0002-7506-4995

2024 11th International Conference on Electrical, Electronic and Computing Engineering (IcETRAN) | 979-8-3503-8699-8/24/$31.00 ©2024 IEEE | DOI: 10.1109/ICETRAN62308.2024.10645092

***Abstract*— Accurate and reliable vital signs monitoring has the potential to detect different health conditions, driver fatigue, or even depression. Contactless approaches for heartbeat and respiration rate monitoring are more comfortable than conventional contact-based monitoring devices. In this paper, heartbeat and breathing data were estimated using Frequency-Modulated Continuous-Wave (FMCW) radar (AWR1843, Texas Instruments, USA) placed underneath the bed on which the participant was lying on the back for 5 minutes. The *Wearable Wellness System* (Smartex, Italy) was used to obtain the reference signal for breathing and heart rate. FMCW data from three participants were acquired during the resting state scenario. First, a slow-time phase correlation method was applied to FMCW data to increase the signal-to-noise ratio. Subsequently, an Adaptive Nonlinear Least Square (ANLS) framework was used to explore the frequency characteristics of the phase signal. Additionally, the Adaptive Notch filter (ANF) removed the second and third breathing harmonics. Finally, the Kalman filter (KF) was applied for better heart rate accuracy. The average root mean square error (RMSE) for estimation from 10-second time windows was 1.66 BPM for the breathing rate estimation and 1.61 BPM for the heart rate estimation.**

***Keywords*— *breathing rate, heart rate, frequency-modulated continuous wave radar, slow-time phase correlation, Adaptive Nonlinear Least Square Framework, Adaptive Notch filter, Kalman filter***

## I. Introduction

Vital signs, such as respiration rate (rate of breathing) and heart rate (rate of heartbeat), are conventionally acquired using contact-based methods involving cables and electrodes placed on the body. However, these approaches have significant drawbacks. Participants often experience discomfort during recordings due to sensor placement, and there is a risk of reduced signal quality due to sensor movement, cable interference, or participant movement [1]. Contactless methods for measuring respiration and heart rate offer promising alternatives to traditional contact approaches. The use of non-intrusive contactless methods to estimate breathing and heart rate shows promising potential for identifying various psycho-physical states, such as detecting abnormal heart rhythms, drowsiness, and stress. Different studies have already explored contactless approaches using radar technology (Doppler radar, Frequency-Modulated Continuous Wave (FMCW) radar, and Ultra-Wideband radar) [2]. Doppler radars offer simplicity and low power consumption but can be affected by reflections from other moving objects. UWB pulse radars provide high spatial resolution but are limited by pulse width and signal intensity. FMCW wide-band radar combines UWB's ranging with CW Doppler's sensitivity and robustness, making it effective for detecting micro-motions and monitoring multiple targets at various ranges. Additionally, FMCW radar is compact, lightweight, energy-efficient, and supports real-time processing, making it more reliable in challenging environments like hospitals and homecare settings. Breathing and heart rate estimation from FMCW data is usually done by using the basic Fast Fourier Transform (FFT) method over time with additional data preprocessing [3-8]. Alizadeh et al. [4] introduced DC compensation before performing FFT in order to qualitatively estimate a phase shift, and they generated three range-time maps for three different regions to explore the environment around the participant and reduce the percentage of the wrong breathing and heart rate estimations. Ahmad et al. [5] suggested finding inter-peak distances in time-domain waveforms of the breathing and heart rate, buffering N maximum FFT spectrum peaks, and clustering them with the dBscan algorithm to provide the most precise breathing and heart rate estimation among all inter-peaks from time-domain signals. Wang et al. [7] applied

This work was financially supported by Novelic d.o.o, Belgrade, Serbia, the Innovation Fund of the Republic of Serbia, innovation voucher, no. 760 and the Ministry of Science, Technological Development, and Innovation of the Republic of Serbia under contract numbers 451-03-65/2024-03/200103 and 451-03-66/2024-03/200223.

adaptive digital beamforming with 3D FFT, introducing azimuth as the third observed dimension to extract the position, breathing, and heart rate of participants. Nonlinear Least Squares (NLS) estimation with Kalman filtering solution was proposed for breathing monitoring using FMCW radar [9]. Wenjie et al. [10] used an Adaptive Notch filter (ANF) to remove higher breathing components and increase the accuracy of heart rate detection from FMCW data.

In this paper, an application of adaptive nonlinear filtering, including Notch, adaptive NLS, and Kalman filter, was used for the breathing and heart rate estimation based on FMCW radar data acquired in a pilot study performed on three back-lying participants. The main contribution of this paper lies in proposing and pilot-testing an algorithm that has the potential to estimate heart rate and breathing rate in real-world scenarios (with the radar positioned beneath the bed) within relatively short time intervals (10 s), offering future potential for near real-time applications.

## II. Method

### A. Principle of FMCW radar

The FMCW radar is a device that generates an electromagnetic signal that has linearly increasing frequency and transmits it into the propagation space via transmitting antennas [11]. FMCW radar receives signals that are reflected from the objects in their field of view. Each FMCW radar unit consists of both transmitting and receiving systems. The primary goal of FMCW radars is to capture high-frequency signals, with a current angular frequency determined by:

$$f(t) = f_c + \frac{BW}{T_{ch}} t = f_c + St \tag{1}$$

where $f_c$ is the starting frequency for the input signal, $BW$ is the bandwidth of the input signal (difference between maximum and minimum frequency), $T_{ch}$ is the period of the chirp signal, while $S$ represents the slope of the ramp, i.e. division of bandwidth and period of the chirp signal.

The current phase of the transmission signal is determined through the integration of the current angular frequency:

$$\phi(t) = \int 2\pi f(t) dt = 2\pi f_c\, t + \pi S t^2 \tag{2}$$

From previous relations, the final equation for the transmitted signal $\boldsymbol{v}_{tx}(t)$ is:

$$v_{tx}(t) = A_1 \cos\big(\phi(t)\big) = A_1 \cos(2\pi f_c t + \pi S t^2) \tag{3}$$

Received signal $\boldsymbol{v}_{rx}(t)$ represents a delayed version of the transmitted signal $\boldsymbol{v}_{tx}(t)$, and its final form is:

$$v_{rx}(t) = A_2 \cos\big(\phi(t-\tau)\big)$$
$$= A_2 \cos(2\pi f_c (t-\tau) + \pi S (t-\tau)^2) \tag{4}$$

where $\tau$ is $2\frac{d}{c}$ and it represents the delay time of the received signal $\boldsymbol{v}_{rx}(t)$, relative to the transmitted signal $\boldsymbol{v}_{tx}(t)$, where $d$ is the distance from the radar to the observed target and $c$ is the speed of light.

Using FFT, phase signal $P(r_k)$ is obtained as [11]:

$$P(r_k) = 2\tan^{-1} \frac{imag(\sum_{n=0}^{N_{fft}-1} v_{RX}(n) e^{-j\frac{2\pi kn}{N}})}{real(\sum_{n=0}^{N_{fft}-1} v_{RX}(n) e^{-j\frac{2\pi kn}{N}})} \tag{5}$$

where $r_k = ck/2BW$, for k = 0, ..., $N_{fft}$-1, $N_{fft}$ is the number of points in which FFT is performed.

### B. Experiment setup and hardware description

During the experiment, FMCW AWR1843 radar was used for data acquisition, including a board for evaluation AWR1843BOOST and a board for data collecting DCA1000EVM (*Texas Instruments*, USA). The number of transmitting antennas $N_{tx}$ was 3, and the number of receiving antennas $N_{rx}$ was 4.

The configuration of FMCW radar was set to the following values: Started Frequency of Chirp signal, $f_c$ – 79 Hz; Idle Time, IT – 40 μs; Analog-to-digital conversion (ADC) sampling time, $T_{ADC}$ – 8 μs; Duration of Chirp signal, $T_{ch}$ – 75 μs; Slope of Chirp signal, S – 30 GHz/μs; Number of Samples per Chirp signal, $N_{ADC}$ – 128; The sampling frequency, $f_s$ – 2000 kHz; Number of Chirp signals per frame, $N_{chirp}$ – 32; Duration of one frame, $T_{frame}$ – 20 ms.

Radar data acquisition was performed using the *mmWaveStudio* software (Texas Instruments, USA). Wearable Wellness System *(WWS, Smartex,* Pisa, Italy) was used to obtain reference breathing and heart rate values. The sampling frequencies of the *WWS* system for breathing and heart rate were 25 Hz and 250 Hz, respectively.

The radar was placed underneath the bed, directly under the participant's chest, at a distance of 35 cm, measured by a laser rangefinder. The rationale for positioning a radar beneath the bed stems from its potential clinical applications (e.g., embedding within hospital beds), ensuring unhindered patient access to the bed compared to a radar placed above it. The experiment was performed on three healthy subjects: ages 26.7±5.23, 1 male, and 2 females. They have signed the informed consent to participate in the study. During the experiment, the participant was lying on the back with the hands next to the body and breathing normally for 5 minutes. This observed dataset is the subset of data acquired in [12].

### C. Algorithm description

Received radar data were archived in .bin files and loaded in a 4D structure with dimensions $N_{adc}$ x $N_{chirp}$ x $N_{rx}$ x $N_{tx}$ =128x32x4x3. The implemented algorithm for breathing and heart rate estimation includes two blocks: Data preprocessing and Data processing block.

The data preprocessing block that is performed on a single radar data frame includes the following steps:

1. Performing FFT (Range FFT, $N_{fft}$ = 128 points, Blackman windowing) over the first dimension of the received signal ($N_{adc}$)
2. Multiplying Range FFT signal with calibration coefficients given by the radar manufacturer
3. Coherent averaging [13] of calibrated signal through all chirps, all transmitting and receiving antennae.
4. Range-time map generation by adding coherent averaged signals to the buffer. The buffer size of 500 x $N_{fft}$ was selected due to the maximum breathing period of $T_{breathing\_max}$=10 s – the first dimension value 500 was calculated as $T_{breathing\_max}$ / $T_{frame}$.

The data processing block that is performed on the full buffer (500 frames) includes the following steps, Fig. 1:

1. Obtaining the observed target range bin as a maximum of all range bins from range-time map magnitude (*max_range*)

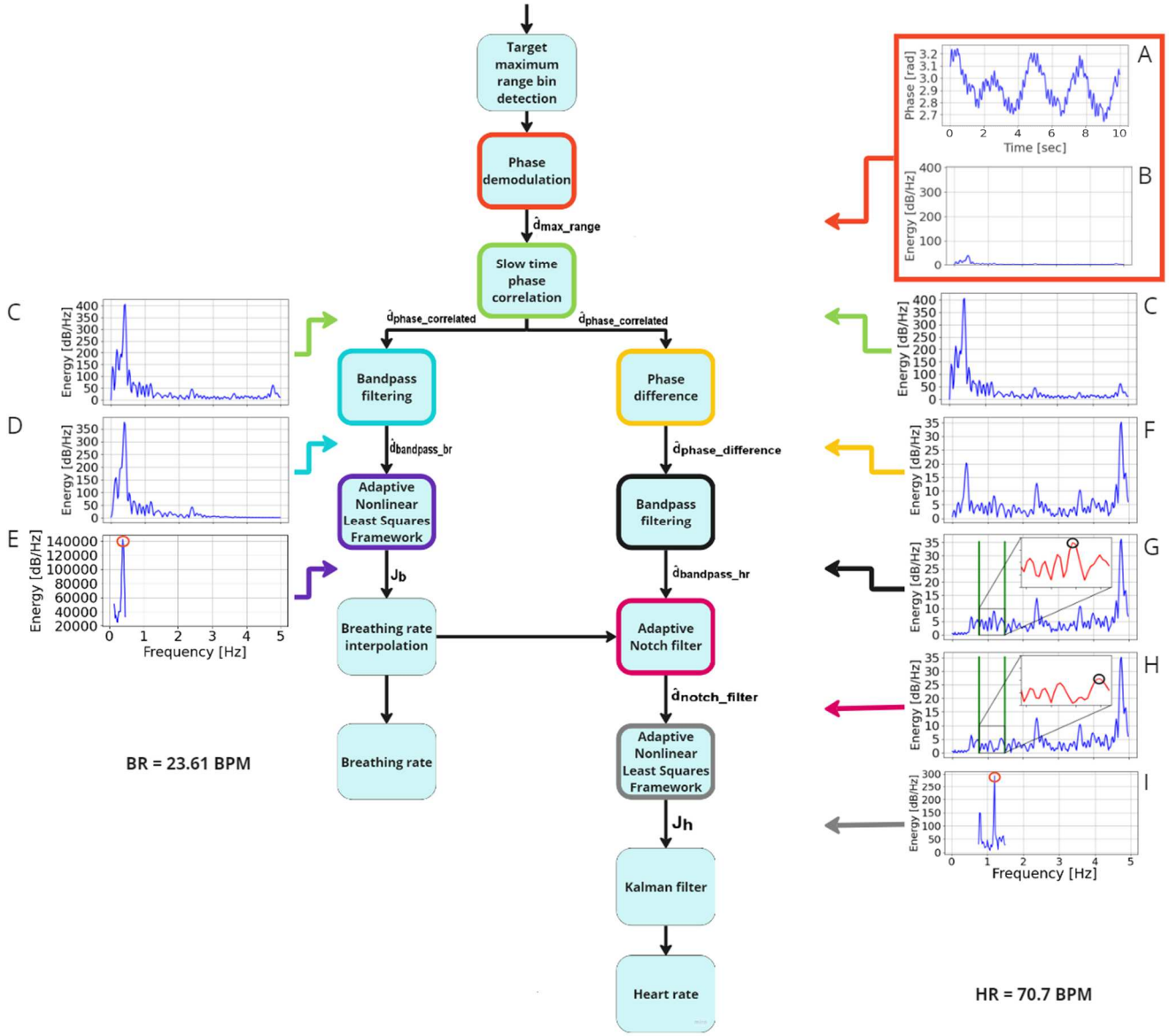


Fig. 1. Block diagram of the Data processing for breathing and heart rate estimation, BR - breathing rate, HR – heart rate

2. Phase demodulation, which includes applying phase calculation (5) and phase unwrapping (removing all „sudden jumps“, i.e. signal changes that are bigger than $2\pi$) over 1D signal, is obtained from the range-time map in *max_range* bin. The result of the demodulated phase is marked as $\hat{d}_{max\_range}$, Fig. 1A and 1B
3. Slow time phase correlation (see Section II C1) over phase demodulated signal and range-time map, Fig. 1C
4. Breathing rate estimation:
    a. Bandpass filtering (Butterworth filter, 10th order, frequency range 0.1 Hz - 3 Hz) [9], $\hat{d}_{bandpass\_br}$, Fig. 1D
    b. Adaptive Nonlinear Least Squares Framework for breathing rate estimation and Breathing rate interpolation (see Section II C3), Fig. 1E
5. Heart rate estimation:
    a. The phase difference of slow time phase correlated signal to suppress the breathing component, which represents the simple and efficient filter, practical for future real-time applications, $\hat{d}_{phase\_difference}$, Fig. 1F
    b. Bandpass filtering (Butterworth filter, 10th order, frequency range 0.5 Hz - 5 Hz) [9], $\hat{d}_{bandpass\_hr}$, Fig. 1G
    c. Adaptive Notch filter (see Section II C2) of the second and third breathing components obtained from step 4b, $\hat{d}_{notch\_filter}$, Fig. 1H
    d. Adaptive Nonlinear Least Squares Framework for heart rate estimation (see Section II C3), Fig. 1I
    e. Kalman filter for the precise heart rate estimation (see Section II C4).

Data load and Data preprocessing block were performed using the *Matlab* R2022a environment, while Data processing block was done in the *Python* environment version 3.10.11 [14].

### *C1. Slow-time Phase Correlation*

An example of the phase-demodulated signal $\hat{d}_{max\_range}$ for a predefined time interval of buffer (500 frames, 10 s) is given in Fig. 1A, while its frequency spectrum is obtained in Fig. 1B.

Due to the radar range resolution (~4 cm) and its proximity to the human body (~35 cm), range-time energy is

spread across a few adjacent range bins, and it is necessary to extract information from them in order to get the better SNR and higher frequency energy, which will lead to better both breathing and heart rate estimation. For the detection of adjacent range bins, a novel slow-time phase correlation processing was proposed in [9], which allows the integration of the vital sign energy of nearby range bins while still preserving its relevant frequency content. Slow-time phase correlation was based on the calculation of the Pearson coefficient $\rho$ for the detected *max_range* and 5 bins above and below it:

$$\rho\left(\hat{d}_{max\_range}, \hat{d}_i\right) = \frac{cov(\hat{d}_{max\_range}, \hat{d}_i)}{\sigma_{\hat{d}_{max\_range}} \sigma_{\hat{d}_i}} \quad (6)$$

where $cov(\hat{d}_{max\_range}, \hat{d}_i)$ represents the covariance between demodulated phase for the *max_range* and *i*-th range bin from it ($\hat{d}_i$) and $\sigma_{\hat{d}_{max\_range}}$ and $\sigma_{\hat{d}_i}$ the corresponding standard deviations. The final demodulated phase signal, $\hat{d}_{phase\_correlated}$, will be equal to the sum of the initial phase demodulated signal $\hat{d}_{max\_range}$ and all phase demodulated signals from range bins with Pearson coefficient higher than 0.90. Therefore, by summing similar range bins, the total observed energy is higher (higher SNR), and vital signs become easier to extract, Fig. 1C.

### *C2. Adaptive Notch Filter*

To precisely extract heart peaks from the NLS estimation spectrum, it is necessary to suppress higher breathing harmonics, which have higher SNR than fundamental heart rate frequency. In the paper [10], the ANF was proposed for this type of filtering due to the narrow stop band and fast attenuation in a band, in comparison with conventional digital filters. The adaptiveness of the ANF filter is reflected in the usage of adaptive Fourier coefficients' tuning, and the implementation of ANF based on a least mean square (LMS) algorithm is given in detail in [14]. Two ANFs were used to remove the second and third breathing harmonics. An example of the frequency spectrum before and after ANF is given in Fig. 1G and 1H, respectively. The circle in the enlarged plot in Fig. 1G presents the third breathing harmonic incorrectly detected as the heart fundamental frequency, while the circle in the enlarged plot in Fig. 1H presents the correctly detected heart fundamental frequency.

### *C3. Adaptive Nonlinear Least Squares Framework*

Nonlinear Least Squares Framework. Gabriel et al. [9] proposed NLS estimation for the modelling of the chest displacement signal as a sum of two sources, breathing and heart source, with $L_b$ and $L_h$ number of harmonics, respectively ($L_b$=3, $L_h$=5). NLS estimation finds the minimum distance between the received signal and the signal model. The cost function for NLS breathing ($J_b$) and heart ($J_h$) estimator can be written as:

$$J_b = \sum_{l=1}^{L_b} \left\| z^H(w_{br} l) \hat{d}_{bandpass\_br} \right\|_2^2 \quad (7)$$

$$J_h = \sum_{l=1}^{L_b} \left\| z^H(w_{hr} l) \hat{d}_{notch\_filter} \right\|_2^2 \quad (8)$$

with $z^H(w_{br}l) = [\ e^{-jw_{start\_br}}\ e^{-(w_{start\_br}+j\Delta_{w_{br}}*1)l}, \ldots, e^{-(w_{start\_br}+j\Delta_{w_{br}}(N_{br}-1))l}\ ]$ and $z^H(w_{hr}l) = [\ e^{-jw_{start\_hr}l}\ e^{-(w_{start\_hr}+j\Delta_{w_{hr}}*1)l}, \ldots, e^{-(w_{start\_hr}+j\Delta_{w_{hr}}(N_{hr}-1))l}\ ]$, where $N_{br}=(BR_{stop}-BR_{start})/BR_{step}$ represents the length of the grid search used for breathing rate estimation, $BR_{stop}$ the last breathing rate in the breathing grid search, $BR_{start}$ the first breathing rate in the breathing grid search, $BR_{step}$ the breathing rate step and $N_{hr}=(HR_{stop}-HR_{start})/HR_{step}$ the length of the grid search used for heart rate estimation, $HR_{stop}$ the last heart rate in the heart grid search and $HR_{start}$ the first heart rate in the heart grid search, $HR_{step}$ the heart rate step, $\Delta_{w_{br}} = 2\pi\Delta_{f_{br}}$, with $\Delta_{f_{br}}=BR_{step}/60$ frequency step within grid search for breathing rate estimation, $\Delta_{w_{hr}}=2\pi\Delta_{f_{hr}}$, with $\Delta_{f_{hr}}=HR_{step}/60$ frequency step within grid search for heart rate estimation, $w_{start\_br}=2\pi f_{start\_br}$, with $f_{start\_br}=BR_{start}/60$, first frequency within grid search for breathing rate estimation and $w_{start\_hr}=2\pi f_{start\_hr}$, with $f_{start\_hr}=HR_{start}/60$ first frequency within heart rate estimation. The cost function is the periodogram power spectral density estimate of $\hat{d}_{bandpass\_br}$ signal for breathing and $\hat{d}_{notch\_filter}$ signal for heart estimator, summed over the $L_b$ and $L_h$ harmonic frequencies. The NLS estimator is implemented using an FFT algorithm and a linear grid search over the discrete frequencies [9].

Adaptive NLS for breathing rate estimation. Grid search for adaptive NLS for breathing rate estimation was set to physiological breathing rate range 6-30 BPM [9], with $BR_{start}=6$ *BPM*, $BR_{stop}=30$ *BPM,* and $BR_{step}=1.5$ *BPM*. In the first frame, where estimation is possible (full buffer), the grid search was set to the whole physiological breathing range. In the following frames, the grid search was limited to 2 $BR_{step}$ below and above the breathing estimation in the previous frame. The position of the maximum value of the breathing cost function $J_b$ from the grid search is the input of the Breathing rate interpolation step. An example of ANLS spectrum estimation over the first grid search for breathing rate estimation (6-30 BPM) is presented in Fig. 1E (the circle marks the peak that corresponds to the breathing rate).

Breathing rate interpolation. The following formula [10] is applied to get the final breathing rate estimation BR:

$$BR = 60 * (k_0 + 1 - \frac{2|J_b(k_0-1)|}{|J_b(k_0+1)|+|J_b(k_0-1)|})\Delta_{f_{br}} \quad (9)$$

where $k_0$ represents the maximum position.

Adaptive NLS for heart rate estimation. Grid search was applied over three ranges: 1) physiological heart rate range 45-90 BPM [9], with $HR_{start}=45$ *BPM*, $HR_{stop}=90$ *BPM* and $HR_{step}=1.5$ *BPM*, 2) physiological heart rate range multiplied by 2 (90-180 BPM), with $HR_{start}=90$ *BPM*, $HR_{stop}=180$ *BPM*, $HR_{step}=1.5$ *BPM*, and 3) physiological heart rate range multiplied by 3 (135-270 BPM), with $HR_{start}=135$ *BPM*, $HR_{stop}=270$ *BPM*, $HR_{step}=1.5$ *BPM*. The position of the maximum values of the heart cost function $J_h$ from the grid search over three ranges is the input of the Kalman filtering step (Section IIC4) that will extract the final heart rate value *HR*. The effect of applying the second and third ranges will be presented in Section IIC4. An example of ANLS spectrum estimation over the first grid search for heart rate estimation (45-90 BPM) is presented in Fig. 1I (the circle marks the peak that corresponds to the heart rate).

### *C4. Kalman filter*

The adaptive NLS for heart rate estimation described in Section IIC3 provides three heart rate values for the time interval of buffer (10 s). Thus, it is necessary to choose which one of the three obtained heart rate values represents the most precise estimation of *HR,* the final heart rate estimation. To obtain this, the Kalman filter, described in [9], is implemented and applied. The Kalman filter represents a recursive Bayesian algorithm. Additionally, it offers adaptability to varying heart

rate variability, preventing inaccuracies caused by interference from sources, low SNR, or ambiguous heart rate estimates resulting from overlapping ranges in grid searches (Section IIC3). Implementation of the Kalman filter and the selection of initial parameters were performed in the same manner as it was presented in [9] ($\rho_a = 2$, $\sigma_{r1} = \sigma_{r2} = \sigma_{r3} = 1.5$, $P_{0,0} = 1000\boldsymbol{I}$).

### D. *Reference signal processing*

The Neurokit2 library [15] was utilized for peak detection in both the respiratory curve and electrocardiogram (ECG) signals acquired by the reference system (WWS). By calculating the intervals between detected peaks and then averaging them within 10-second windows, reference values for breathing and heart rates were extracted.

## III. Results and Discussion

Fig. 2-3 represents the breathing rate and heart rate for 5 minutes of the first participant lying on the back during normal breathing. Fig. 2-3 illustrate results obtained both from the radar and reference sensor, with blue and red lines, respectively. Breathing and heart rate, which were processed using overlapped sliding windows with 10 s duration and 0.02 s of overlap, are shown with thicker red and blue lines. Averaged breathing and heart rate, with 30 s averaging window duration and 0.02 s of overlap, are shown with thinner red and blue lines. Gray parts of the radar signal represent results with a low quality, where breathing and heart rate estimates are not within ±3 standard deviations (STD) of the reference signal. In Fig. 2, a red rectangle denotes a part of the experiment where the reference measurements were shown to have extreme value changes within a short time interval. These changes are not representative of the actual breathing activity of the participants but indicate poor-quality reference measurements and, therefore, should not be used for further radar estimation evaluation. The percentage of data where breathing rate reference was excluded is a total of 8.89% of collected data, while the percentage of excluded heart rate reference data was 6.01%. In Fig. 3, the gray parts of the radar heart rate results are consequences of the noisy radar signal and its low SNR. Low SNR leads to poor breathing estimation and wrong filtering of the second and third breathing components. Thus, the NLS estimator cannot extract the precise heart rate frequency due to the mentioned reason, and the accuracy of the heart rate estimation drops.

Table I and Table II present the metrics of breathing rate and heart rate estimation, respectively, for three participants. Table rows are the following: root mean square error (RMSE), mean and STD values both for Radar and Reference estimation and Bland Altman Analysis [16] with three parameters: Bias, Lower Limit of Agreement (LLoA), and Upper Limits of Agreement (ULoA). For each participant, noisy radar data sequences were observed with the criteria that the radar results are within ±3 STD of the reference signal, and the results in both cases (for noisy and noise-free radar data) are presented in Table I and II to observe the quality of the radar dynamic tracking (*REMOVED NOISY RADAR DATA* raw indicates the percentage of data that was removed because of the noise). Observing Table I and Table II, it can be concluded that the best dynamic tracking of the breathing rate was obtained for the third participant, with RMSE of 1.25 BPM and 20.88% removed parts, while the best dynamic tracking of the heart rate was obtained for the first participant, with RMSE of 0.48 BPM and 16.92% removed parts. Furthermore, the most accurate agreement between Radar and Reference, in terms of the mean values, was obtained for the first participant, both for the breathing and heart rate estimation, with Bias of -0.6 BPM and -0.09 BPM, respectively. The low SNR could be the reason for the lower performance of other participants. Furthermore, Kalman filter parameters, specifically heart rate, could affect the results in terms of sudden jumps in heart rate radar estimation. Although these tables do not show better results in comparison with a previous study that used Kalman filtering ([9] –average RMSE of breathing rate estimation for static scenario – 0.43 BPM and average RMSE of heart rate estimation for static scenario – 0.76 BPM), the main advantage of this work is using shorter sliding window for radar processing. In this work, a 10 s sliding window and 0.02 s overlap were used, while the previous study [9] used a 30 s sliding window and 1 s overlap.

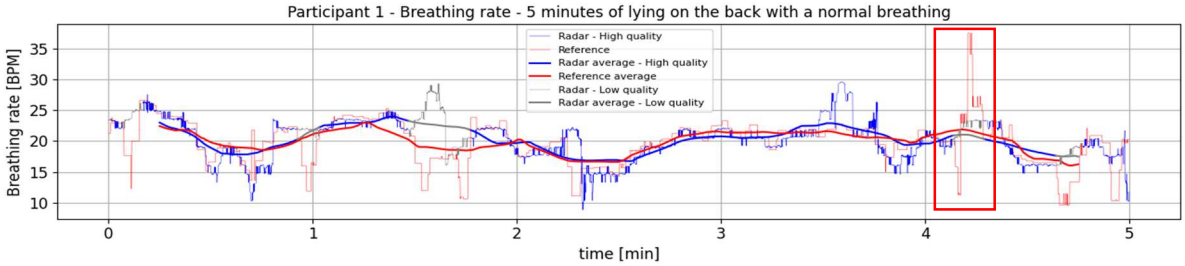


Fig. 2. Breathing rate for 5 minutes of the first participant (low quality of the reference values – red rectangle)

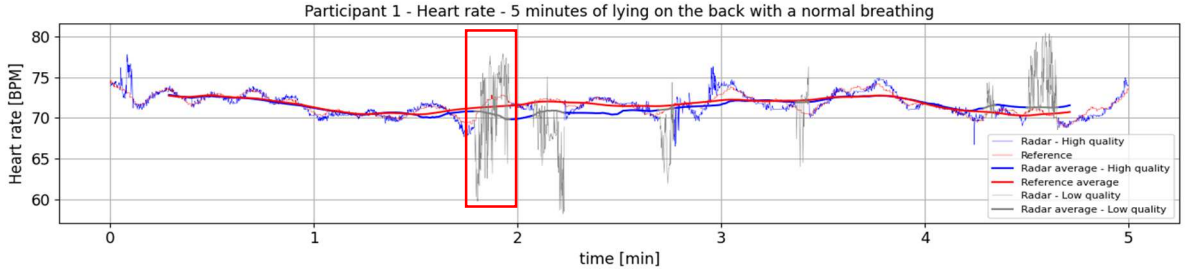


Fig. 3. Heart rate for 5 minutes of the first participant (low quality of the radar signal – red rectangle)

TABLE I. THE BREATHING RATE ESTIMATION

| METRICS/ NO. PART. | | 1 | | 2 | | 3 | |
|---|---|---|---|---|---|---|---|
| REMOVED NOISY RADAR DATA [%] | | 0 | 12.23 | 0 | 10.98 | 0 | 20.88 |
| RMSE [BPM] | | 3.01 | 1.98 | 2.84 | 1.74 | 4.09 | 1.25 |
| Radar Mean ± STD [BPM] | | 20.2 ± 3.4 | 19.7 ± 3.1 | 18.1 ± 2.7 | 18.6 ± 1.9 | 21.4 ± 4.1 | 22.6 ± 1.8 |
| Reference Mean ± STD [BPM] | | 20.1 ± 3.1 | 20.3 ± 2.8 | 19.4 ± 1.7 | 19.3 ± 1.7 | 23.1 ± 1.8 | 23.3 ± 1.7 |
| Bland Altman Analysis [BPM] | Bias | 0.09 | -0.6 | -1.29 | -0.68 | -1.7 | -0.65 |
| | LLoA | -5.8 | -4.3 | -6.2 | -3.8 | -9 | -2.7 |
| | ULoA | 6 | 3.1 | 3.7 | 2.5 | 5.6 | 1.5 |

TABLE II. THE HEART RATE ESTIMATION

| METRICS/ NO. PART. | | 1 | | 2 | | 3 | |
|---|---|---|---|---|---|---|---|
| REMOVED NOISY RADAR DATA [%] | | 0 | 16.92 | 0 | 11.30 | 0 | 38.26 |
| RMSE [BPM] | | 1.72 | 0.48 | 3.18 | 2.52 | 14.94 | 1.81 |
| Radar Mean ± STD [BPM] | | 71.5 ± 2.1 | 71.5 ± 1.3 | 63.6 ± 2.63 | 63.7 ± 2.31 | 69.4 ± 12.4 | 60.8 ± 2.1 |
| Reference Mean ± STD [BPM] | | 71.6 ± 1.1 | 71.7 ± 1.1 | 65.1 ± 3.1 | 65.1 ± 2.9 | 61.1 ± 2.3 | 61.3 ± 2.5 |
| Bland Altman Analysis [BPM] | Bias | -0.15 | -0.09 | -1.51 | -1.36 | 8.27 | -0.48 |
| | LLoA | -3.5 | -1 | -7 | -5.5 | -16 | -3.9 |
| | ULoA | 3.2 | 0.83 | 4 | 2.8 | 33 | 3 |

However, with the larger dataset containing more subjects, potentially better reference sensors, and adjustments of Kalman filter parameters, further investigations could result in better performances, both for breathing and heart rate estimation and tracking.

The presented research focused on near real-time HR/BR estimation and comparing the results obtained from all available data and non-noisy data. The trade-off between the continuity of HR/BR estimation and the error is evident since removing noisy radar data decreases the error but creates gaps in the HR/BR signal. Interpolation of the signals or a separate estimation algorithm for noisy radar data could be part of future research, building upon the existing results and providing measurements suitable for HRV and BRV analysis.

## IV. CONCLUSION

In this paper, adaptive nonlinear filtering was applied to FMCW radar data over a 10 s window to obtain both breathing and heart rate. Furthermore, the Kalman filter was used to detect peaks in the NLS spectrum precisely over grid searches for heart rate estimation. For the breathing and heart rate estimation, the average RMSE was 1.66 BPM and 1.61 BPM, respectively. Better results may be attributed to a combination of factors, including a low SNR in the radar signal, suboptimal algorithm parameters, particularly those of the Kalman filter, and the quality of the reference signal. To enhance future investigations, potential improvements could involve fine-tuning algorithm parameters, adopting a different reference system, automatic removal of the low-quality radar signal parts, considering the BRV and HRV data analysis and collecting additional radar data from a larger and more diverse group of participants.

## REFERENCES


[1] M. Kebe, R. Gadhafi, B. Mohammad, M. Sanduleanu, H. Saleh, M. Al-Qutayri, „Human vital signs detection methods and potential using radars: A review", *Sensors*, vol. 20, no. 5, p. 1454, 2020.

[2] M. Liebetruth, K. Kehe, D. Steinritz, S. Sammito, „Systematic Literature Review Regarding Heart Rate and Respiratory Rate Measurement by Means of Radar Technology," *Sensors*, vol. 24, no. 3, p. 1003, 2024.

[3] G. Beltrao, M. Alaee-Kerahroodi, U. Schroeder, D. Tatarinov, „Nonlinear least squares estimation for breathing monitoring using FMCW radars," in *Proc. 18th Eur. Radar Conf. (EuRAD), London, 5-7 April,* pp. 241–244, 2022.

[4] M. Alizadeh, G. Shaker, J. C. M. De Almeida, P. P. Morita, and S. Safavi-Naeini, „Remote monitoring of human vital signs using mm-wave FMCW radar," *IEEE Access*, vol. 7, pp. 54958–54968, 2019.

[5] A. Ahmad, J. C. Roh, D. Wang, A. Dubey, „Vital signs monitoring of multiple people using a FMCW millimeter-wave sensor," in *Proc. IEEE Radar Conf., Oklahoma City, 23-27 April,* pp. 1450–1455, 2018.

[6] S. Lim, G. S. Jang, W. Song, B. H. Kim, D. H Kim, „Non-contact vital signs monitoring of a patient lying on surgical bed using beamforming FMCW radar", *Sensors*, vol. 22, no. 21, p. 8167, 2022.

[7] W. Wang, Y. Wang, M. Zhou, W. Nie, „A novel vital sign sensing algorithm for multiple people detection based on FMCW radar", *IEEE Asia-Pacific Microwave Conference (APMC)*, *Hong Kong*, *8-11 December*, pp. 1104-1106, 2020.

[8] Y. Zhao, V. Sark, M. Krstic, E. Grass, „Multi-target vital signs remote monitoring using mmWave FMCW radar", *IEEE Microwave Theory and Techniques in Wireless Communications (MTTW)*, *Riga*, 7-*8 October*, pp. 290-295, 2021.

[9] B. Gabriel, M.R. Shankar, M. Alaee-Kerahroodi, U. Schroeder, D. Tatarinov, „Adaptive Nonlinear Least Squares Framework for Contactless Vital Sign Monitoring," *IEEE Access*, vol. 71, 1969-1710, 2023.

[10] W. Lv, W. He, H. Lin, J. Miao, „Non-Contact Monitoring of Human Vital Signs Using FMCW Milimeter Wave Radar in the 120 GHz Band," *Sensors*, 2732, 2021.

[11] S.I. Merril, „Introduction to Radar Systems," *MacGraw-Hill*, New York City, United States, 2001.

[12] L. Jugović, I. Vajs, M. B. Atanasijević, M. Stojanović, M. M. Janković, „Convolutional Neural Network Model in Human Motion Detection Based on FMCW Radar Signals", *E-business technologies conference proceedings*, *Belgrade, 15-17 June*, vol. 3, pp. 127-13, 2023.

[13] A. Zyweck, R. E. Bogner, „Coherent averaging of range profiles. In *Proceedings International Radar Conference"*, *Alexandria*, *8-11 May*, pp. 456-461, 1995.

[14] Y. Xiao, Y. Tadokoro, „LMS-based notch filter for the estimation of sinusoidal signals in noise ", *Signal Processing,* vol. 46, pp. 223-231, 1995.

[15] G. Van Rossum and F. L. Drake, „Python 3 Reference Manual*"*, *Scotts Valley, CA: CreateSpace*, 2009.

[16] J. M. Bland, D. G. Altman, „Statistical methods for assessing agreement between two methods of clinical measurement," *Lancet*, vol. 1, pp. 307–310, 1986.